CLIMATE CHANGE

Rainfall regimes of the Green Sahara

Jessica E. Tierney,[1]* Francesco S. R. Pausata,[2] Peter B. deMenocal[3]

During the "Green Sahara" period (11,000 to 5000 years before the present), the Sahara desert received high amounts of rainfall, supporting diverse vegetation, permanent lakes, and human populations. Our knowledge of rainfall rates and the spatiotemporal extent of wet conditions has suffered from a lack of continuous sedimentary records. We present a quantitative reconstruction of western Saharan precipitation derived from leaf wax isotopes in marine sediments. Our data indicate that the Green Sahara extended to 31°N and likely ended abruptly. We find evidence for a prolonged "pause" in Green Sahara conditions 8000 years ago, coincident with a temporary abandonment of occupational sites by Neolithic humans. The rainfall rates inferred from our data are best explained by strong vegetation and dust feedbacks; without these mechanisms, climate models systematically fail to reproduce the Green Sahara. This study suggests that accurate simulations of future climate change in the Sahara and Sahel will require improvements in our ability to simulate vegetation and dust feedbacks.

INTRODUCTION

During the early Holocene epoch [11,000 to 5000 years before the present (yr B.P.)], the hyperarid Sahara was transformed into a mesic landscape, with widespread grasslands, variable tree cover, large permanent lakes, and extensive river drainage networks. Evidence for this "Green Sahara" interval comes from paleolake deposits, pollen, and archaeological remains, indicating that humans inhabited, hunted, and gathered deep within the present-day desert (1–3). The Green Sahara was the most recent of a succession of wet phases paced by orbital precession that extends back to the late Miocene (4). When the precessional cycle approaches perihelion during boreal summer, the increase in insolation drives a strong land-sea temperature gradient over North Africa that strengthens the African monsoon, bringing rainfall deep into the Sahara (5). Climate model experiments demonstrate that oceanic and land surface feedbacks can amplify this initial response, resulting in even wetter conditions (6, 7). These feedbacks may also result in abrupt shifts between wet and dry regimes (7, 8), and some sedimentary records suggest that the Green Sahara terminated within centuries around 5000 yr B.P. (9–11). Given the marked and expansive nature of the climate changes associated with the Green Sahara, it is a useful case study of how gradual external climate forcing in arid environments can result in rapid, nonlinear responses, a particularly instructive lesson in our currently warming world.

The timing and magnitude of the rainfall changes that established the Green Sahara are still not well characterized. Our best indicators to date come from pollen records recovered from paleolake deposits in the desert. These data suggest that the Sahara hosted steppe, savannah, and wooded grassland environments, with tropical plants migrating as far as 24°N (12–14). These shifts correspond to an increase in precipitation across the Sahara and Sahel of 500 mm/year or more (14–16). Likewise, sedimentological and lake-level studies suggest that permanent paleolakes extended at least to 28°N (17), associated with increases in rainfall of ca. 300 to 900 mm/year (18–20). However, most of the lacustrine deposits from which these data are derived are poorly dated and discontinuous. Thus, these quantitative estimates generally apply only to the early or middle Holocene and do not give a clear picture of how the Green Sahara evolved through time and space.

Here, we used leaf wax biomarkers preserved in marine sediment cores to create a continuous, spatiotemporal reconstruction of precipitation rates in western Sahara. Our reconstruction spans the last 25,000 years, describing both the onset and termination of the Green Sahara as well as conditions during the Last Glacial Maximum and the deglaciation. We used a transect of gravity cores from the West African margin that span the full meridional breadth of the Sahara (19°N to 32°N; Fig. 1). To reconstruct precipitation, we used paired measurements of the carbon and hydrogen isotopic composition of leaf waxes ($\delta^{13}C_{wax}$ and δD_{wax}) and a Bayesian regression approach (see Materials and Methods and the Supplementary Materials). δD_{wax} is an excellent tracer for the hydrogen isotopic composition of precipitation (δD_P) (21). However, large changes in vegetation, such as those that occurred during the Green Sahara, have secondary effects on the signal (21). Correcting δD_{wax} for vegetation impacts using paired $\delta^{13}C_{wax}$ improves the inference of δD_P (see fig. S1 and the Supplementary Materials) (22, 23). In turn, δD_P has a strong ($r = -0.72$) log-normal relationship with the amount of rainfall in western Sahara (see fig. S2, Materials and Methods, and the Supplementary Materials), allowing us to quantitatively infer precipitation rates.

RESULTS

The δD_P and inferred precipitation rates from our core sites place important new constraints on the spatiotemporal evolution of the Green Sahara as well as the magnitude of rainfall change (Figs. 2 and 3A). The Green Sahara period (ca. 11,000 to 5000 yr B.P.) emerges at every site as the time interval with the most depleted δD_P and the highest inferred rainfall rates (Fig. 2). Median rainfall rates during the Green Sahara, across all sites, were 640 mm/year, but there is substantial spatiotemporal variability (1σ range, 250 to 1670 mm/year; Fig. 2B). This represents a remarkable difference from modern-day rainfall rates in western Sahara, which range from 35 to 100 mm/year. However, these numbers agree with the pollen and lake-level estimates (see discussion above), and they are consistent with the proposed landscape: a mix of grasslands, shrubs, and tropical elements. Grasslands dominate landscapes at precipitation rates from 300 to 800 mm/year in Africa (24) and Sudanian group taxa, which require rainfall rates between 500 and 1500 mm/year, expanded to 25°N (14). Thus, in general, our precipitation rate estimates confirm the interpretation that a seasonal tropical climate dominated most regions of North Africa during the Green Sahara time (14).

[1]Department of Geosciences, University of Arizona, 1040 East Fourth Street, Tucson, AZ 85721, USA. [2]Department of Meteorology, Stockholm University, Stockholm, Sweden. [3]Lamont Doherty Earth Observatory, Palisades, NY 10964, USA.
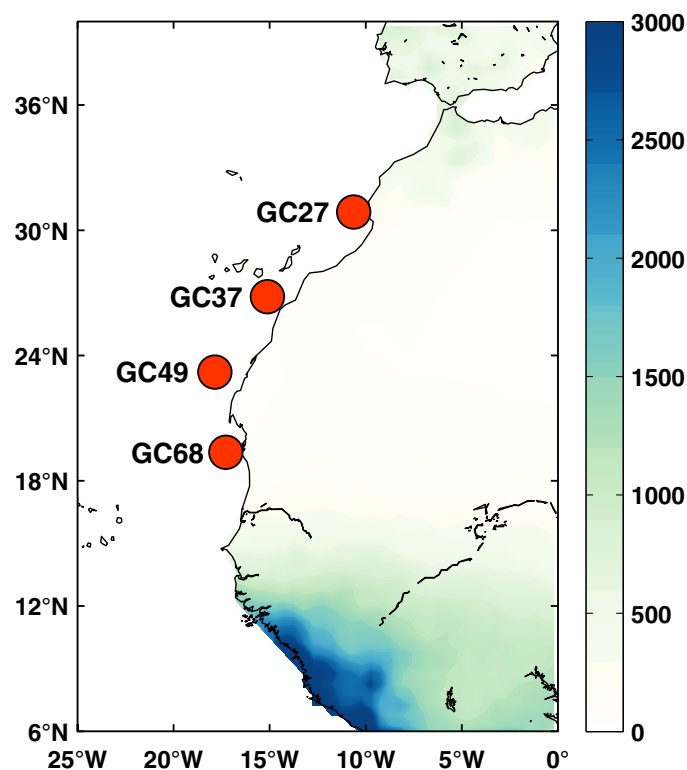*Corresponding author. Email: jesst@email.arizona.edu

Fig. 1. Location of the sediment cores used in this study and modern mean annual precipitation rates (in millimeters per year) (60). These cores were collected as part of the Changing Holocene Environments Eastern Tropical Atlantic (CHEETA) *R/V Oceanus* cruise (OCE437-7) in 2007. Site GC27: 30.88°N, 10.63°W, 1258-m water depth; GC37: 26.816°N, 15.118°W, 2771-m water depth; GC49: 23.206°N, 17.854°W, 2303-m water depth; GC68: 19.363°N, 17.282°W, 1396-m water depth.

Notably, we observe very wet conditions as far as 31°N (Figs. 2B and 3A). Our northernmost site is located offshore from Cape Ghir, Morocco: a region that presently experiences a December to March rainy season typical of the Mediterranean. However, it is likely that most of the observed increase is monsoonal. Modeling experiments using either prescribed or interactive vegetation suggest that the changes in atmospheric circulation during the early Holocene were large enough to advect monsoonal moisture up to 30°N (25–27). In addition, analysis of an idealized mid-Holocene Green Sahara simulation (27) indicates that 90% of the annual increase at 31°N occurs during June to September (fig. S3). It is therefore feasible that, at the peak of the Green Sahara, monsoonal moisture inundated the entire western Saharan region. However, the mid-Holocene simulation also shows a strong weakening of the Azores high in winter, raising the possibility that a larger increase in winter precipitation occurred than those simulated (fig. S3). A dual-season increase may be partly responsible for the exceptionally high rainfall rates that we infer at 31°N (median, 1280 mm/year; 1σ range, 560 to 2550 mm/year).

DISCUSSION

Spatiotemporal variability and abrupt change during the Green Sahara

Our rainfall reconstructions clarify both the timing and variability of high precipitation rates during the Green Sahara. Peak rainfall typically occurred between 11,000 and 6000 yr B.P., but conditions evolved

differently by latitude. In general, our data show that the Green Sahara was relatively restricted at higher latitudes (31°N) and lasted longer at lower latitudes (Fig. 3A). At our lowest latitude site (19°N), humid conditions were established early during the deglaciation, with median rainfall rates during the Bølling-Allerød period (B/A) interstadial (14,500 to 12,800 yr B.P.) of 1430 mm/year (1σ range, 623 to 2740 mm/year) (Figs. 2B and 3A). δD_{wax} records from the Sahel and tropical West Africa similarly show relatively depleted values during the B/A (23, 28), indicating that, at low latitudes in western Africa, fully humid conditions were established before the deglaciation was complete. In contrast, our more northerly sites show that Green Sahara conditions were not established until the early Holocene (Fig. 3A). Bioturbation forward modeling suggests that humid conditions terminated early at 31°N [median value, 6500 yr B.P.; 6.5 thousand years ago (ka)] as compared with the other three sites to the south (m = 5.0, 5.3, and 5.3 ka, respectively; figs. S4 and S5). This generally supports the hypothesis that the termination of the Green Sahara was time-transgressive, with areas farther away from the epicenter of the West African monsoon experiencing earlier aridification as the monsoon retreated (23); however, we do not see a clear time transgression in the termination dates between 19°N and 27°N. A time-transgressive response does not preclude the existence of a regionally abrupt termination of high precipitation rates. Our bioturbation modeling suggests that the end of the Green Sahara was likely abrupt (occurring within a few hundred years) at all four of our core sites (see the Supplementary Materials), in agreement with analyses of dust data from the same sites (10) and other δD_{wax}-based records in East Africa (11).

In addition to a wet B/A event, our lowest latitude site (19°N) records pronounced drying during the Younger Dryas (YD) (12,800 to 11,500 yr B.P.). Although the YD is generally a dry interval between 23°N and 31°N, it is not readily distinguishable from the B/A or the rest of the deglacial sequence because of the prevalence of dry conditions before the event (Fig. 3A). Similarly, Heinrich event 1 (17,500 to 14,500 yr B.P.), which is associated with dry conditions throughout the East African and Indian monsoon domains (29), is not prominently featured in any of our precipitation records from western Sahara (Fig. 3A), most likely because rainfall rates were low and the West African monsoon did not extend to the latitudes of our sites (19°N to 31°N) during late glacial times.

An early Holocene pause in Green Sahara conditions

We observe a prominent reduction in precipitation during the early Holocene—around 8000 yr B.P. (8 ka)—at the sites spanning 19°N to 23°N (Figs. 2B and 3A). This 8 ka dry period is also seen in a nearby δD_{wax} record from the Sahel (15°N) (28), in leaf wax and lake-level records from East Africa (11, 30), and in numerous lake-level reconstructions from across the Sahara (fig. S6) (1). We do not observe a clear 8 ka pause between 27°N and 31°N in our data, and a survey of existing records indicates that, although it may be expressed inland at these latitudes, the duration of the event is short (fig. S6). One explanation for the weak expression of the 8 ka dry period at these latitudes is that winter rainfall contributions obscured the event (see discussion above).

The 8 ka pause in Green Sahara conditions appears to have lasted for a millennium or more. Bioturbation forward modeling indicates that a dry period of at least 1000 years is needed to explain the duration of the event at our sites (fig. S4). In addition, other proxy data across Africa suggest extended and severe drying at this time (fig. S6). The archaeological record from the Sahara provides further compelling evidence of a prolonged 8 ka dry period. In particular, the duration of the
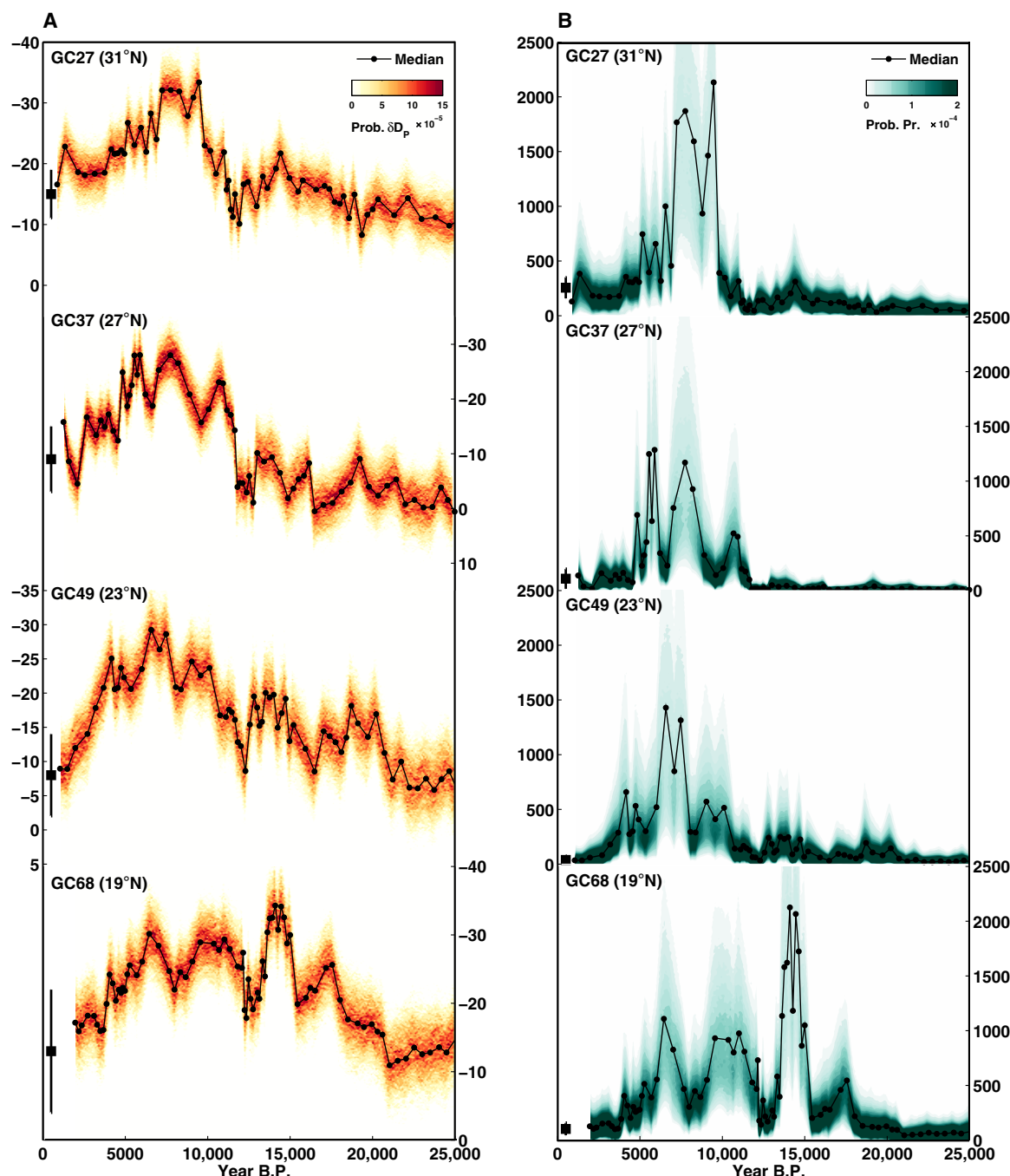
Fig. 2. δD$_{wax}$-inferred δD$_P$ (A) and mean annual precipitation (in millimeters per year) (B) at each core site. Black lines indicate median values; colors indicate posterior probability distributions. Black squares with error bars denote modern mean annual observational values and SDs [from the Online Isotopes in Precipitation Calculator (61) for δD$_P$ and Global Precipitation Climatology Centre version 6 (60) for precipitation]. Note that, because our δD$_{wax}$ precipitation regression is logarithmic, the uncertainty of our inferred precipitation rates increases at higher precipitation amounts; thus, probability densities are more broadly distributed during wet intervals.

8 ka pause in our precipitation reconstructions aligns with evidence from the Gobero site in Niger (17°N), where extensive radiocarbon dating indicates that there was an interruption in occupation from 8150 to 7150 yr B.P., during which time a lake nearby dried up (Fig. 4) (31). The 8 ka pause also begins slightly before a prominent mid-Holocene dip in Saharan demographics, estimated from a density of over 1000 radiocarbon dates from archaeological sites (Fig. 4) (32).

The inferred demographic delay relative to the climatic event is expected as populations adjust to new environmental conditions; a similar delay is seen in the population response to the onset of Green Sahara conditions in the early Holocene (32).

The archaeological record further suggests that the 8 ka pause is associated with a distinctive change in lifestyle. At Gobero, the humans occupying the site before the 8 ka pause were hunter-fisher-gatherers,
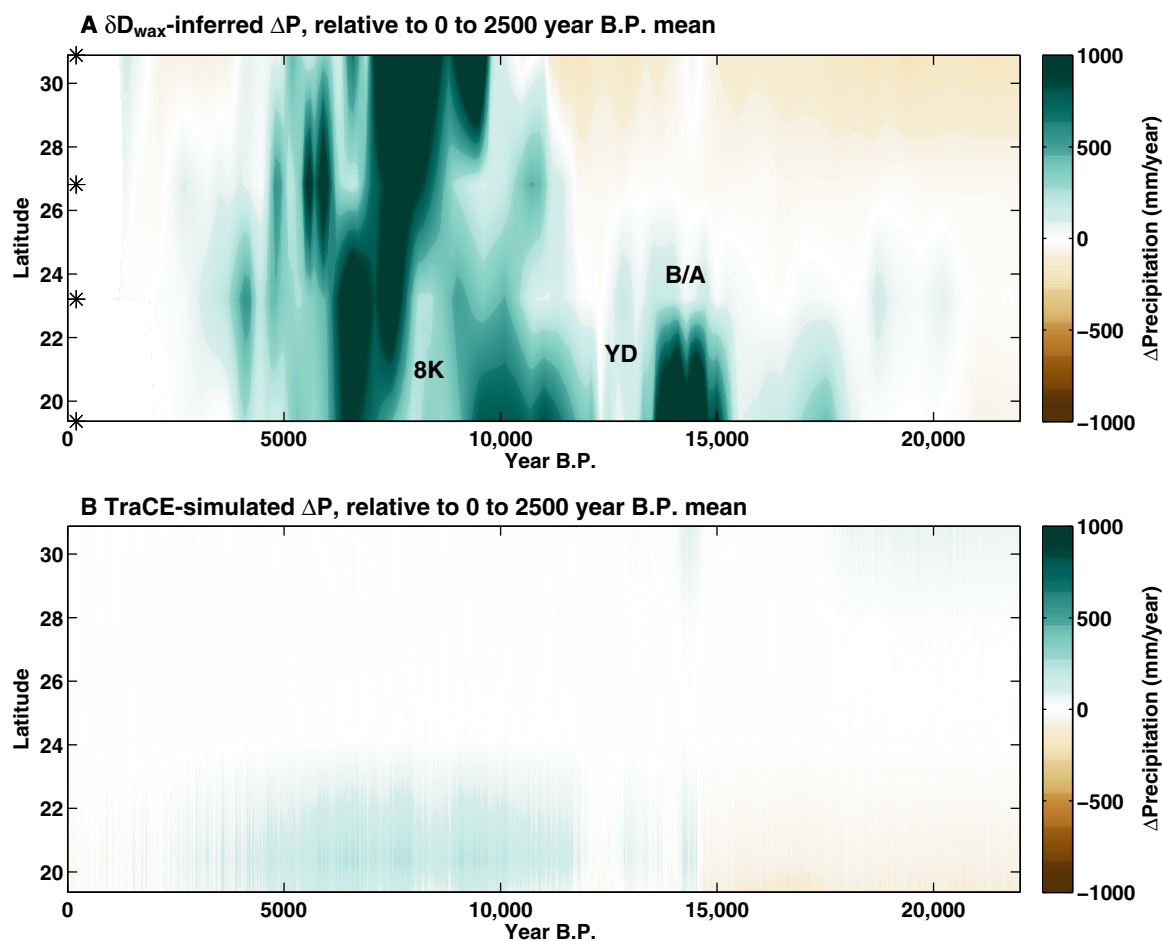
Fig. 3. Hovmöller diagrams of proxy-inferred and model-simulated precipitation in western Sahara. (**A**) δD_{wax}-inferred mean annual precipitation. Asterisks denote the latitudinal locations of the core sites. (**B**) Mean annual precipitation from the TraCE experiment, conducted with the CCSM3 climate model (44). B/A, Bølling/Allerød period; YD, Younger Dryas; 8K, 8 ka "pause."

whereas the humans that occupied the site after the pause had a more diversified diet that included cattle husbandry (31). More generally, widespread adoption of pastoralism in the Sahara (the raising of cattle, the "cattle cult," and the practice of dairying) occurs after the 8 ka pause (33, 34). The temporary deterioration of climate conditions at 8 ka in the Sahara may have been an impetus to abandon hunting and gathering in favor of cattle herding, a more resilient strategy in the face of a fluctuating climate (35).

What might have caused this mid-Holocene pause in humid conditions? The beginning of the 8 ka pause is roughly coeval with the "8.2 event" in the North Atlantic, a widespread cooling event in the Northern Hemisphere (36) caused by the sudden drainage of Lake Agassiz and Lake Ojibway (37) and a subsequent slowdown of the Atlantic Meridional Overturning Circulation. However, although the 8.2 event only lasted for a couple of hundred years (38), and its expression in the Northern Hemisphere rarely exceeds 500 years (36), our data suggest a dry period lasting ca. 1000 years. This leaves us with two possibilities: (i) the 8 ka arid phase was coincident with but unrelated to the 8.2 cooling event, or (ii) the 8 ka pause was directly related to the 8.2 event and climatic feedbacks amplified its impact and prolonged its duration in the Sahara. Regarding the first possibility, one hypothesis is that, at peak Green Sahara conditions, the monsoonal system extended so far

north that it left the West African tropics drier. Some mid-Holocene (6 ka) model simulations do show evidence of drier conditions below ca. 10°N in response to a northward shift in the monsoon (27, 39). This may explain the prolonged nature of the 8 ka event in both lake-level and δD_{wax} data from tropical West Africa (5°N) (23) but cannot reasonably explain the presence of the 8 ka pause at ca. 23°N (Fig. 3A and fig. S6).

Although speculative, a direct relationship between the 8.2 event and the 8 ka pause fits better with the available data. The onset of the 8 ka pause agrees reasonably well with known events associated with the 8.2 event (Fig. 4). Furthermore, the presence of the B/A and YD events at our lower latitude site suggests that North Atlantic forcing affects the West African monsoon system. As we discuss in further detail below, vegetation and dust feedbacks likely played a large role in maintaining high precipitation rates during the Green Sahara. Whereas there is no evidence for increased dust flux near 8 ka (10), there is a fluctuation in the richness and abundance of vegetation types around this time (14). A short-lived drying caused by the 8.2 event may have reduced vegetative cover, leading to changes in albedo that prolonged the drying and made it more difficult for the Green Sahara ecosystem to recover. Thorough testing of this hypothesis requires high-resolution pollen records from the Sahara, as well as model
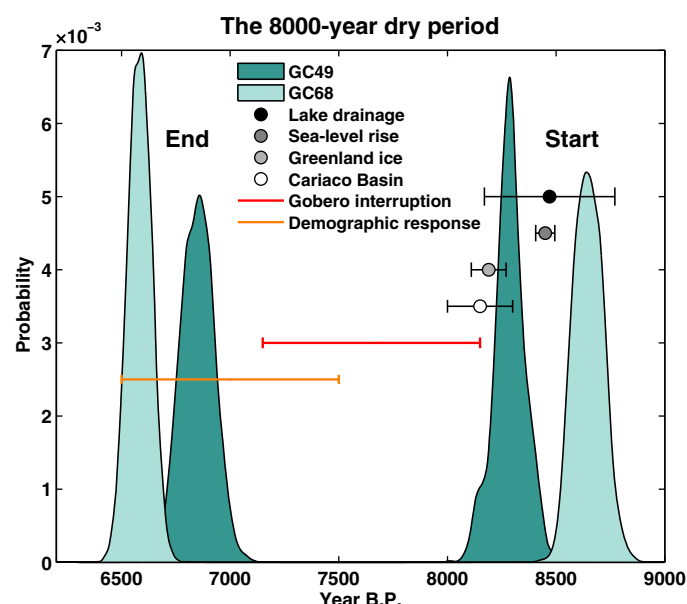
Fig. 4. The 8 ka pause in Green Sahara conditions. Green areas denote the probability distributions of the start and end of the 8 ka dry period at sites GC49 (23°N) and GC68 (19°N), on the basis of the inferred locations in the core (from bioturbation modeling) for an abrupt beginning and end, and Monte Carlo iteration of age model uncertainties. Black and gray dots with error bars represent the mean and 1σ ages for climatic events associated with the 8.2 cooling event in the Northern Hemisphere, including (i) the timing of the drainage of Lake Agassiz and Lake Ojibway (37); (ii) the timing of an abrupt rise in sea level, detected in the Netherlands (62); (iii) the duration of the 8.2 event in the Greenland ice cores (38); and (iv) the duration of the response in Cariaco Basin grayscale data (63). Shown in red is the timing and duration of a prolonged interruption in the occupation of the Gobero site by humans (31). The yellow bar indicates a Sahara-wide demographic decline (32).

simulations to assess the sensitivity of the Green Sahara to millennial-scale perturbation.

The importance of vegetation and dust feedbacks
Our data indicate that Green Sahara rainfall rates were ca. 10 times higher than present-day "Desert Sahara" rates. With some notable exceptions (40), climate model simulations do not predict these high rainfall rates, nor do they indicate that the Green Sahara extended as far as 31°N (39, 41, 42). For example, the TraCE-21ka (Simulation of Transient Climate Evolution over the past 21,000 years) transient experiment (43, 44) shows a muted response in the western Sahara, with an average increase in rainfall of 124 mm/year at ca. 20°N (Fig. 3B). There is no simulated increase in precipitation above 24°N (Fig. 3B).

The Paleoclimate Modeling Intercomparison Project (PMIP) mid-Holocene (6 ka) simulations also drastically underestimate both the magnitude and spatial extent of rainfall in western Sahara (Fig. 5). In the PMIP experiments, a number of climate models were run both with and without dynamic vegetation modules (Fig. 5). Although in general the simulations with dynamic vegetation produced a greater increase in precipitation than their paired simulations without vegetation, dynamic vegetation was not a panacea. It is virtually certain (>99.5% probability) that rainfall rates across the Green Sahara as a whole were higher than the multimodel mean simulated changes in the PMIP experiments, consistent with previous assessments based on pollen data (41, 42).

The systematically low simulated rainfall amounts suggest that there is a missing component to the forcings or the feedbacks involved. As the primary forcing (changes in orbital configuration) is well known, it is most likely that the relevant feedback mechanisms are not adequately accounted for. Inadequate vegetation feedbacks have long been suspected and investigated as the explanation for low simulated rainfall rates (7, 40, 45). Recently, Pausata et al. (27) demonstrated that dust feedbacks can further enhance the intensity and northward penetration of the African monsoon under Green Sahara conditions. In their experiments, when the model was forced with both prescribed vegetation and reduced dust concentrations, the monsoon reached ca. 31°N. Given just the prescribed vegetation, the monsoon reached ca. 26°N, whereas orbital forcing alone only moved the monsoon ca. 200 km north (to ca. 16°N) relative to the preindustrial simulation (27). The "Green Sahara–reduced dust" (GS-RD) experiment from Pausata et al. (27) is the only simulation out of the 31 investigated here that produces a magnitude of rainfall increase comparable to the δD_{wax}-inferred values, along with high rainfall rates extending to 31°N (Fig. 5). In this simulation, the prescription of Green Sahara vegetation is responsible for most of the changes, accounting for ca. 80% of the increase in rainfall at 19°N and ca. 65% of the increase in rainfall between 23°N and 31°N. This suggests that the strength of the vegetation feedbacks—either via albedo feedbacks or through moisture feedbacks (8, 46)—may be too weak in PMIP models with dynamic vegetation schemes, preventing models from simulating realistically vegetated conditions and correspondingly higher rainfall rates. Implementation of dynamic albedo schemes provides noticeable improvement, but simulated rainfall rates are still low when compared to proxy evidence (45).

Although vegetation feedbacks are important, the additional impact of reduced dust is key to producing rainfall rates on par with the proxy data, and this mechanism becomes increasingly important at higher latitudes (up to 35%) (Fig. 5). Several modern-day modeling studies show that increased dust aerosols over West Africa tend to decrease precipitation along the northern edge of the monsoon (47, 48), supporting the importance of dust in suppressing monsoon convection. However, the effect is relatively small (10% reduction) (47), and other studies have proposed that dust may actually enhance the strength of the monsoon (49). The simulations of Pausata et al. (27) demonstrate that the presence of Green Sahara vegetation markedly alters this picture. Reducing dust with preindustrial (non-vegetated) conditions results in no increases in rainfall, primarily because the change in albedo is very small (27). In contrast, the changes in surface albedo between a Green Sahara and a dusty Green Sahara are substantial and directly affect heating at the surface, resulting in an enhanced monsoon and increases in rainfall (27). Hence, the interaction between vegetation and dust changes varies as a function of climate background state, and in the Green Sahara case, reduced dust acts as a strong positive feedback on the hydrological cycle.

SUMMARY AND CONCLUSIONS
In summary, our δD_{wax}-inferred precipitation reconstructions from the West African margin provide a continuous and quantitative view of rainfall rates for the last 25,000 years, including the Green Sahara interval. Our data reveal important spatiotemporal aspects of this remarkable change in hydroclimate, including an extreme northward incursion of the African monsoon (31°N) from 9.5 ka to 7 ka and the presence of a prominent pause in Green Sahara conditions near 8 ka. The millennium-long duration of the 8 ka pause matches exceptionally well with the archaeological record and provides a climatic
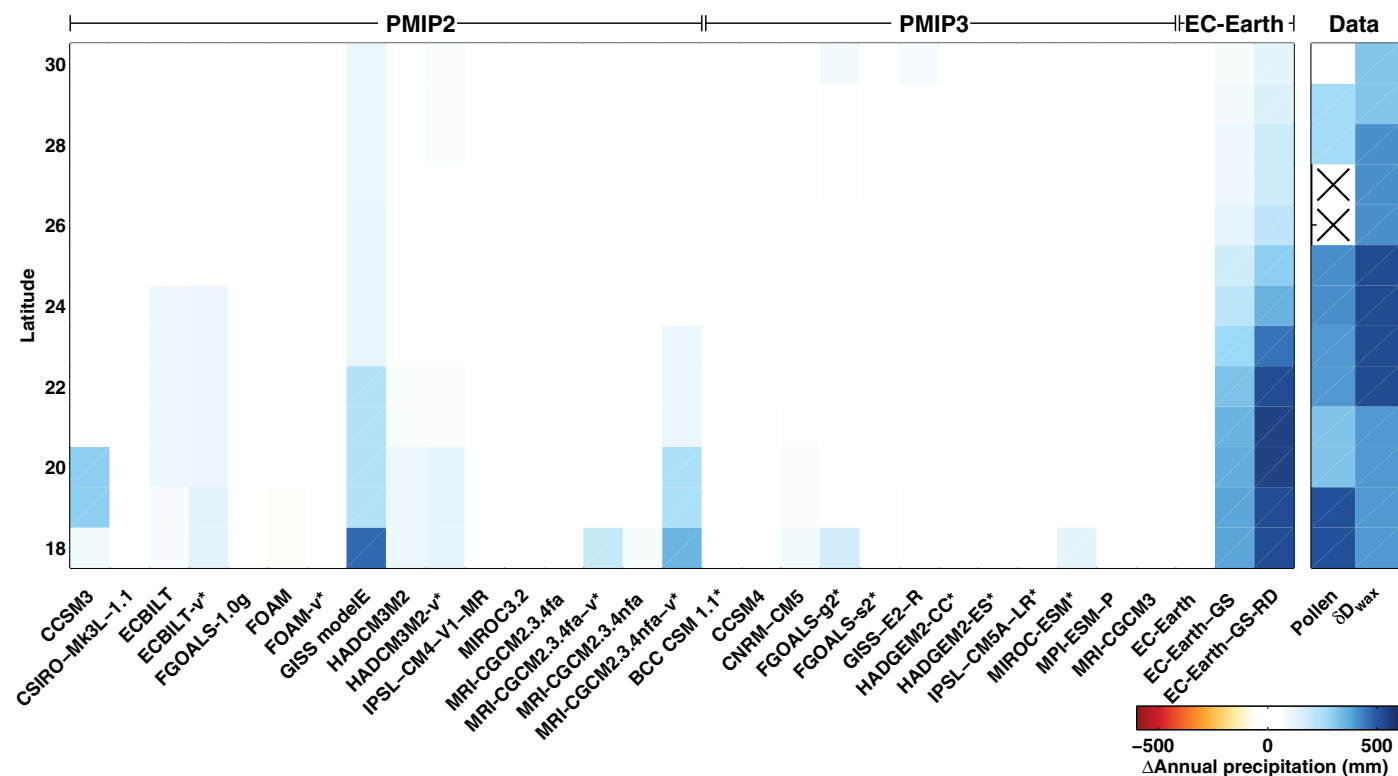
Fig. 5. Comparison between paleoclimate data and model simulations of mid-Holocene (6 ka) climate in the western Sahara. Model data represent 6 ka anomalies (relative to preindustrial control simulations) for land grid cells closest to the Atlantic coast along the given latitudes (y axis). Asterisks next to the model names (x axis) denote models with a dynamic vegetation module. PMIP2 and PMIP3 indicate models participating in the Paleoclimate Intercomparison Project Phase 2 and 3, respectively. The EC-Earth simulations are from the study by Pausata et al. (27). The data shown include both pollen-inferred precipitation data (16) and leaf wax–inferred precipitation data (this study). To overcome the paucity of data in the western Sahara, the pollen data represent average values across the entirety of North Africa for the given latitudes. X denotes no data available for the given latitude.

explanation for the observed occupational patterns, demographic response, and lifestyle changes of Neolithic humans. We speculate that the 8.2 cooling in the Northern Hemisphere initiated the pause and that land surface feedbacks prolonged it. Likewise, we show that strong vegetation and dust feedbacks are necessary to explain the magnitude and intensity of the African monsoon during the Green Sahara. The prominent role of dust in forcing the Green Sahara agrees with 20th century analyses of Sahel rainfall, suggesting that dust feedbacks are as important as sea surface temperature and vegetation changes in driving observed historical trends (50). Furthermore, the features seen in our data, including the rapid termination of the Green Sahara and the prolonged 8 ka pause, are consistent with the idea that the Sahara has multiple stable states, mediated by vegetation or dust feedbacks (8, 51).

The climate models used in the PMIP2 and PMIP3 experiments systematically fail to reproduce the Green Sahara, likely because vegetation feedbacks are weak (or nonexistent), and the simulations do not account for the concomitant changes in desert dust. The PMIP3 experiments were conducted with the same climate models used for CMIP5 (Coupled Model Intercomparison Project Phase 5) future climate scenarios; thus, there are direct implications for our ability to simulate future rainfall changes in the Sahara and Sahel, and perhaps other arid and hyperarid regions. There is currently no consensus across models as to whether precipitation in West Africa will increase or decrease in response to a rise in anthropogenic greenhouse gases (52–54). Our study suggests that advances in the simulation of vegetation and dust feedbacks may clarify future climate change in this

region and also help identify whether the West African monsoon system will pass a "tipping point" (55), as it did so dramatically during the Green Sahara.

MATERIALS AND METHODS
Paleoclimate reconstructions

δD_P and precipitation reconstructions were derived from analyses on four sediment cores along the West African margin (Fig. 1). Radiocarbon dating of planktonic foraminifera provided chronological constraint (see the Supplementary Materials for a list of dates and fig. S7 for the age-depth models for each core). The cores were sampled for leaf wax analyses every 3 to 4 cm. Sediments were extracted, purified, and analyzed for the carbon and hydrogen composition of leaf waxes according to previously established methods (see the Supplementary Materials for further details) (11). Bayesian regression modeling was used to develop quantitative inferences of δD_P and precipitation from the leaf wax isotopes. δD_{wax} is a reliable tracer of δD_P, but it can be overprinted by changing vegetation types; in particular, C_4 grasses have a very different apparent fractionation (isotopic difference between δD_P and δD_{wax}; $\varepsilon_{water-wax}$) compared to C_3 shrubs and trees (21). However, $\delta^{13}C_{wax}$ tracks the balance between C_3 and C_4 plant types (56) and therefore may be used to correct the δD_{wax} signal for the impact of changing vegetation on $\varepsilon_{water-wax}$ (22). Using modern core top sediments collected during the CHEETA cruise, we validated the use of δD_{wax} and $\delta^{13}C_{wax}$ to quantitatively infer δD_P (see fig. S1B and

the Supplementary Materials). We then used the downcore δD_{wax} and $\delta^{13}C_{wax}$ measurements to infer past δD_P, after correcting for ice volume impacts on δD_{wax} that occur on glacial-interglacial time scales (see the Supplementary Materials).

δD_{wax} has been widely used as a qualitative indicator for past changes in aridity in Africa because the "amount effect" is the primary control on the isotopic composition of precipitation in most regions (11, 57). At our coastal, arid core sites along western Sahara, the amount effect on δD_P is pronounced and the rainfall derives exclusively from the Atlantic Ocean, making it an ideal locale to attempt quantitative inference of precipitation from δD_P. Observations and isotopic reanalyses suggest that δD_P scales nonlinearly with precipitation rate (fig. S2) such that we may develop a regression between the logarithm of mean annual precipitation and leaf wax–inferred δD_P using core top data. We used Bayesian statistics to both develop this regression and apply it to the δD_P time series, to propagate uncertainties related to both the determination of the regression parameters and the inference of δD_P from δD_{wax} (see the Supplementary Materials).

Bioturbation of marine sediments can affect the apparent timing and duration of rapid climate changes. To analyze the effect of bioturbation on key transitions in our data, we used the TURBO2 forward model (58) to approximate the characteristics of our time series. The forward modeling allows us to constrain the probable timing of the end of the Green Sahara and further suggests that the termination of humid conditions was abrupt (see fig. S4 and the Supplementary Materials). It also suggests that the millennium-long duration of the 8 ka pause at sites GC49 and GC68 cannot be explained by bioturbation (see fig. S4 and the Supplementary Materials). For further details regarding the analytical techniques used to produce the reconstructions, see the Supplementary Materials.

Climate model experiments

We used output from the following: (i) the PMIP2 and PMIP3 mid-Holocene (6 ka) and preindustrial (0 ka) experiments, publicly available online at the Earth System Grid (http://pcmdi9.llnl.gov/); (ii) the TraCE-21ka, a fully coupled, transient simulation conducted with the National Center for Atmospheric Research Community Climate System Model version 3 (CCSM3) (43, 44); and (iii) the prescribed vegetation and dust experiments conducted with the EC-Earth model (27). The PMIP simulations and EC-Earth mid-Holocene control experiments were forced with the same changes in boundary conditions, which include orbital forcing and greenhouse gases (59). The vegetation and the dust concentrations were assumed identical to the preindustrial climate. Two additional idealized experiments were performed with EC-Earth, in which Saharan land cover is set to shrub ("Green Sahara" experiment) and, additionally, dust concentrations ("Green Sahara–Reduced Dust" experiment) were reduced by as much as 80% on the basis of recent estimates of Saharan dust flux reduction during the mid-Holocene (9, 10). The TraCE simulation uses a complete suite of changing boundary conditions for the last 21,000 years, including changes in orbital, greenhouse gas, ice sheet, and freshwater forcings. See the Supplementary Materials for further details on the model simulations and analyses, including a list and description of the models used.

SUPPLEMENTARY MATERIALS

Supplementary Materials and Methods

REFERENCES AND NOTES

1. F. Gasse, Hydrological changes in the African tropics since the Last Glacial Maximum. *Quat. Sci. Rev.* **19**, 189–211 (2000).
2. P. Hoelzmann, B. Keding, H. Berke, S. Kröpelin, H.-J. Kruse, Environmental change and archaeology: Lake evolution and human occupation in the Eastern Sahara during the Holocene. *Palaeogeogr. Palaeoclimatol. Palaeoecol.* **169**, 193–217 (2001).
3. R. Kuper, S. Kröpelin, Climate-controlled Holocene occupation in the Sahara: Motor of Africa's evolution. *Science* **313**, 803–807 (2006).
4. P. B. deMenocal, Plio-Pleistocene African climate. *Science* **270**, 53–59 (1995).
5. J. E. Kutzbach, Monsoon climate of the early Holocene: Climate experiment with the Earth's orbital parameters for 9000 years ago. *Science* **214**, 59–61 (1981).
6. J. E. Kutzbach, Z. Liu, Response of the African monsoon to orbital forcing and ocean feedbacks in the middle Holocene. *Science* **278**, 440–443 (1997).
7. M. Claussen, C. Kubatzki, V. Brovkin, A. Ganopolski, P. Hoelzmann, H.-J. Pachur, Simulation of an abrupt change in Saharan vegetation in the mid-Holocene. *Geophys. Res. Lett.* **26**, 2037–2040 (1999).
8. V. Brovkin, M. Claussen, V. Petoukhov, A. Ganopolski, On the stability of the atmosphere-vegetation system in the Sahara/Sahel region. *J. Geophys. Res. Atmos.* **103**, 31613–31624 (1998).
9. P. B. deMenocal, J. Ortiz, T. Guilderson, J. Adkins, M. Sarnthein, L. Baker, M. Yarusinsky, Abrupt onset and termination of the African Humid Period: Rapid climate responses to gradual insolation forcing. *Quat. Sci. Rev.* **19**, 347–361 (2000).
10. D. McGee, P. B. deMenocal, G. Winckler, J. B. W. Stuut, L. I. Bradtmiller, The magnitude, timing and abruptness of changes in North African dust deposition over the last 20,000 yr. *Earth Planet. Sci. Lett.* **371–372**, 163–176 (2013).
11. J. E. Tierney, P. B. deMenocal, Abrupt shifts in Horn of Africa hydroclimate since the Last Glacial Maximum. *Science* **342**, 843–846 (2013).
12. J. C. Ritchie, C. H. Eyles, C. V. Haynes, Sediment and pollen evidence for an early to mid-Holocene humid period in the eastern Sahara. *Nature* **314**, 352–355 (1985).
13. D. Jolly, I. C. Prentice, R. Bonnefille, A. Ballouche, M. Bengo, P. Brenac, G. Buchet, D. Burney, J.-P. Cazet, R. Cheddadi, T. Edorh, H. Elenga, S. Elmoutaki, J. Guiot, F. Laarif, H. Lamb, A.-M. Lezine, J. Maley, M. Mbenza, O. Peyron, M. Reille, I. Reynaud-Farrera, G. Riollet, J. C. Ritchie, E. Roche, L. Scott, I. Ssemmanda, H. Straka, M. Umer, E. Van Campo, S. Vilimumbalo, A. Vincens, M. Waller, Biome reconstruction from pollen and plant macrofossil data for Africa and the Arabian peninsula at 0 and 6000 years. *J. Biogeogr.* **25**, 1007–1027 (1998).
14. C. Hély, A.-M. Lézine, Holocene changes in African vegetation: Tradeoff between climate and water availability. *Clim. Past* **10**, 681–686 (2014).
15. O. Peyron, D. Jolly, P. Braconnot, R. Bonnefille, J. Guiot, D. Wirrmann, F. Chalié, Quantitative reconstructions of annual rainfall in Africa 6000 years ago: Model-data comparison. *J. Geophys. Res. Atmos.* **111**, D24110 (2006).
16. P. J. Bartlein, S. P. Harrison, S. Brewer, S. Connor, B. A. S. Davis, K. Gajewski, J. Guiot, T. I. Harrison-Prentice, A. Henderson, O. Peyron, I. C. Prentice, M. Scholze, H. Seppä, B. Shuman, S. Sugita, R. S. Thompson, A. E. Viau, J. Williams, H. Wu, Pollen-based continental climate reconstructions at 6 and 21 ka: A global synthesis. *Clim. Dyn.* **37**, 775–802 (2011).
17. A.-M. Lézine, C. Hély, C. Grenier, P. Braconnot, G. Krinner, Sahara and Sahel vulnerability to climate changes, lessons from Holocene hydrological data. *Quat. Sci. Rev.* **30**, 3001–3012 (2011).
18. H.-J. Pachur, P. Hoelzmann, Paleoclimatic implications of late quaternary lacustrine sediments in Western Nubia, Sudan. *Quat. Res.* **36**, 257–276 (1991).

19. F. Mees, D. Verschuren, R. Nijs, H. Dumont, Holocene evolution of the crater lake at Malha, Northwest Sudan. *J. Paleolimnol.* **5**, 227–253 (1991).

20. P. Hoelzmann, H.-J. Kruse, F. Rottinger, Precipitation estimates for the eastern Saharan palaeomonsoon based on a water balance model of the West Nubian Palaeolake Basin. *Glob. Planet. Change* **26**, 105–120 (2000).

21. D. Sachse, I. Billault, G. J. Bowen, Y. Chikaraishi, T. E. Dawson, S. J. Feakins, K. H. Freeman, C. R. Magill, F. A. McInerney, M. T. J. van der Meer, P. Polissar, R. J. Robins, J. P. Sachs, H.-L. Schmidt, A. L. Sessions, J. W. C. White, J. B. West, A. Kahmen, Molecular paleohydrology: Interpreting the hydrogen-isotopic composition of lipid biomarkers from photosynthesizing organisms. *Annu. Rev. Earth Planet. Sci.* **40**, 221–249 (2012).

22. J. A. Collins, E. Schefuß, S. Mulitza, M. Prange, M. Werner, T. Tharammal, A. Paul, G. Wefer, Estimating the hydrogen isotopic composition of past precipitation using leaf-waxes from western Africa. *Quat. Sci. Rev.* **65**, 88–101 (2013).

23. T. M. Shanahan, N. P. McKay, K. A. Hughen, J. T. Overpeck, B. Otto-Bliesner, C. W. Heil, J. King, C. A. Scholz, J. Peck, The time-transgressive termination of the African Humid Period. *Nat. Geosci.* **8**, 140–144 (2015).

24. K. Guan, E. F. Wood, K. K. Caylor, Multi-sensor derivation of regional vegetation fractional cover in Africa. *Remote Sens. Environ.* **124**, 653–665 (2012).

25. H. Renssen, V. Brovkin, T. Fichefet, H. Goosse, Simulation of the Holocene climate evolution in Northern Africa: The termination of the African Humid Period. *Quat. Int.* **150**, 95–102 (2006).

26. J. H. C. Bosmans, S. S. Drijfhout, E. Tuenter, L. J. Lourens, F. J. Hilgen, S. L. Weber, Monsoonal response to Mid-Holocene orbital forcing in a high resolution GCM. *Clim. Past* **8**, 723–740 (2012).

27. F. S. R. Pausata, G. Messori, Q. Zhang, Impacts of dust reduction on the northward expansion of the African monsoon during the Green Sahara period. *Earth Planet. Sci. Lett.* **434**, 298–307 (2016).

28. E. M. Niedermeyer, E. Schefuß, A. L. Sessions, S. Mulitza, G. Mollenhauer, M. Schulz, G. Wefer, Orbital-and millennial-scale changes in the hydrologic cycle and vegetation in the western African Sahel: Insights from individual plant wax δD and $\delta^{13}C$. *Quat. Sci. Rev.* **29**, 2996–3005 (2010).

29. J. C. Stager, D. B. Ryves, B. M. Chase, F. S. R. Pausata, Catastrophic drought in the Afro-Asian monsoon region during Heinrich event 1. *Science* **331**, 1299–1302 (2011).

30. Y. Garcin, V. F. Schwab, G. Gleixner, A. Kahmen, G. Todou, O. Séné, J.-M. Onana, G. Achoundong, D. Sachse, Hydrogen isotope ratios of lacustrine sedimentary *n*-alkanes as proxies of tropical African hydrology: Insights from a calibration transect across Cameroon. *Geochim. Cosmochim. Acta* **79**, 106–126 (2012).

31. P. C. Sereno, E. A. A. Garcea, H. Jousse, C. M. Stojanowski, J.-F. Saliège, A. Maga, O. A. Ide, K. J. Knudson, A. M. Mercuri, T. W. Stafford Jr., T. G. Kaye, C. Giraudi, I. M. N'siala, E. Cocca, H. M. Moots, D. B. Dutheil, J. P. Stivers, Lakeside cemeteries in the Sahara: 5000 years of Holocene population and environmental change. *PLOS ONE* **3**, e2995 (2008).

32. K. Manning, A. Timpson, The demographic response to Holocene climate change in the Sahara. *Quat. Sci. Rev.* **101**, 28–35 (2014).

33. S. Di Lernia, Building monuments, creating identity: Cattle cult as a social response to rapid environmental changes in the Holocene Sahara. *Quat. Int.* **151**, 50–62 (2006).

34. J. Dunne, R. P. Evershed, M. Salque, L. Cramp, S. Bruni, K. Ryan, S. Biagetti, S. di Lernia, First dairying in green Saharan Africa in the fifth millennium BC. *Nature* **486**, 390–394 (2012).

35. B. E. Barich, *Droughts, Food and Culture* (Springer, 2002), pp. 209–223.

36. E. J. Rohling, H. Pälike, Centennial-scale climate cooling with a sudden cold event around 8,200 years ago. *Nature* **434**, 975–979 (2005).

37. D. C. Barber, A. Dyke, C. Hillaire-Marcel, A. E. Jennings, J. T. Andrews, M. W. Kerwin, G. Bilodeau, R. McNeely, J. Southon, M. D. Morehead, J.-M. Gagnon, Forcing of the cold event of 8,200 years ago by catastrophic drainage of Laurentide lakes. *Nature* **400**, 344–348 (1999).

38. E. R. Thomas, E. W. Wolff, R. Mulvaney, J. P. Steffensen, S. J. Johnsen, C. Arrowsmith, J. W. C. White, B. Vaughn, T. Popp, The 8.2 ka event from Greenland ice cores. *Quat. Sci. Rev.* **26**, 70–81 (2007).

39. P. Braconnot, S. Otto-Bliesner, S. Harrison, S. Joussaume, J.-Y. Peterchmitt, A. Abe-Ouchi, M. Crucifix, E. Driesschaert, T. Fichefet, C. D. Hewitt, M. Kageyama, A. Kitoh, A. Laîné, M.-F. Loutre, O. Marti, U. Merkel, G. Ramstein, P. Valdes, S. L. Weber, Y. Yu, Y. Zhao, Results of PMIP2 coupled simulations of the Mid-Holocene and Last Glacial Maximum– Part 1: Experiments and large-scale features. *Clim. Past* **3**, 261–277 (2007).

40. M. Claussen, V. Gayler, The greening of the Sahara during the mid-Holocene: Results of an interactive atmosphere-biome model. *Glob. Ecol. Biogeogr. Lett.* **6**, 369–377 (1997).

41. P. Braconnot, S. P. Harrison, M. Kageyama, P. J. Bartlein, V. Masson-Delmotte, A. Abe-Ouchi, B. Otto-Bliesner, Y. Zhao, Evaluation of climate models using palaeoclimatic data. *Nat. Clim. Change* **2**, 417–424 (2012).

42. S. P. Harrison, P. J. Bartlein, K. Izumi, G. Li, J. Annan, J. Hargreaves, P. Braconnot, M. Kageyama, Evaluation of CMIP5 palaeo-simulations to improve climate projections. *Nat. Clim. Change* **5**, 735–743 (2015).

43. F. He, "Simulating transient climate evolution of the last deglaciation with CCSM3," thesis, University of Wisconsin–Madison, Madison, WI (2011).

44. Z. Liu, B. L. Otto-Bliesner, F. He, E. C. Brady, R. Tomas, P. U. Clark, A. E. Carlson, J. Lynch-Stieglitz, W. Curry, E. Brook, D. Erickson, R. Jacob, J. Kutzbach, J. Cheng, Transient simulation of last deglaciation with a new mechanism for Bølling-Allerød warming. *Science* **325**, 310–314 (2009).

45. F. S. E. Vamborg, V. Brovkin, M. Claussen, The effect of a dynamic background albedo scheme on Sahel/Sahara precipitation during the mid-Holocene. *Clim. Past* **7**, 117–131 (2011).

46. J. G. Charney, Dynamics of deserts and drought in the Sahel. *Q. J. R. Meteorol. Soc.* **101**, 193–202 (1975).

47. M. P. Marcella, E. A. B. Eltahir, The role of mineral aerosols in shaping the regional climate of West Africa. *J. Geophys. Res. Atmos.* **119**, 5806–5822 (2014).

48. Z. Ji, G. Wang, J. S. Pal, M. Yu, Potential climate effect of mineral aerosols over West Africa. Part I: Model validation and contemporary climate evaluation. *Clim. Dyn.* **46**, 1223–1239 (2016).

49. K. M. Lau, K. M. Kim, Y. C. Sud, G. K. Walker, A GCM study of the response of the atmospheric water cycle of West Africa and the Atlantic to Saharan dust radiative forcing. *Ann. Geophys.* **27**, 4023–4037 (2009).

50. M. Yoshioka, N. M. Mahowald, A. J. Conley, W. D. Collins, D. W. Fillmore, C. S. Zender, D. B. Coleman, Impact of desert dust radiative forcing on Sahel precipitation: Relative importance of dust compared to sea surface temperature variations, vegetation changes, and greenhouse gas warming. *J. Clim.* **20**, 1445–1467 (2007).

51. K. Yu, P. D'Odorico, A. Bhattachan, G. S. Okin, A. T. Evan, Dust-rainfall feedback in West African Sahel. *Geophys. Res. Lett.* **42**, 7563–7571 (2015).

52. I. M. Held, T. L. Delworth, J. Lu, K. L. Findell, T. R. Knutson, Simulation of Sahel drought in the 20th and 21st centuries. *Proc. Natl. Acad. Sci. U.S.A.* **102**, 17891–17896 (2005).

53. K. H. Cook, E. K. Vizy, Coupled model simulations of the West African monsoon system: Twentieth- and twenty-first-century simulations. *J. Clim.* **19**, 3681–3703 (2006).

54. I. Niang, O. C. Ruppel, M. A. Abdrabo, A. Essel, C. Lennard, J. Padgham, P. Urquhart, in *Climate Change 2014: Impacts, Adaptation, and Vulnerability*, P. Dube, N. Leary, Eds. (Cambridge Univ. Press, 2014).

55. T. M. Lenton, H. Held, E. Kriegler, J. W. Hall, W. Lucht, S. Rahmstorf, H. J. Schellnhuber, Tipping elements in the Earth's climate system. *Proc. Natl. Acad. Sci. U.S.A.* **105**, 1786–1793 (2008).

56. J. W. Collister, G. Rieley, B. Stern, G. Eglinton, B. Fry, Compound-specific $\delta^{13}C$ analyses of leaf lipids from plants with differing carbon dioxide metabolisms. *Org. Geochem.* **21**, 619–627 (1994).

57. E. Schefuß, S. Schouten, R. R. Schneider, Climatic controls on central African hydrology during the past 20,000 years. *Nature* **437**, 1003–1006 (2005).

58. M. H. Trauth, TURBO2: A MATLAB simulation to study the effects of bioturbation on paleoceanographic time series. *Comput. Geosci.* **61**, 1–10 (2013).

59. K. E. Taylor, R. J. Stouffer, G. A. Meehl, A summary of the CMIP5 experiment design. *PCDMI Rep* 33 (2009).

60. U. Schneider, A. Becker, P. Finger, A. Meyer-Christoffer, B. Rudolf, M. Ziese, *GPCC Full Data Reanalysis Version 6.0 at 0.5°: Monthly Land-Surface Precipitation from Rain-Gauges Built on GTS-Based and Historic Data* (Federal Ministry of Transport and Digital Infrastructure, 2011).

61. G. J. Bowen, J. Revenaugh, Interpolating the isotopic composition of modern meteoric precipitation. *Water Resour. Res.* **39**, 1299 (2003).

62. M. P. Hijma, K. M. Cohen, Timing and magnitude of the sea-level jump preluding the 8200 yr event. *Geology* **38**, 275–278 (2010).

63. K. A. Hughen, J. T. Overpeck, L. C. Peterson, S. Trumbore, Rapid climate changes in the tropical Atlantic region during the last deglaciation. *Nature* **380**, 51–54 (1996).

64. P. J. Reimer, E. Bard, A. Bayliss, J. W. Beck, P. G. Blackwell, C. B. Ramsey, C. E. Buck, H. Cheng, R. L. Edwards, M. Friedrich, P. M. Grootes, T. P. Guilderson, H. Haflidason, I. Hajdas, C. Hatté, T. J. Heaton, D. L. Hoffmann, A. G. Hogg, K. A. Hughen, K. F. Kaiser, B. Kromer, S. W. Manning, M. Niu, R. W. Reimer, D. A. Richards, E. M. Scott, J. R. Southon, R. A. Staff, C. S. M. Turney, J. van der Plicht, IntCal13 and Marine13 radiocarbon age calibration curves 0–50,000 years cal BP. *Radiocarbon* **55**, 1869–1887 (2013).

65. C. B. Ramsey, Radiocarbon calibration and analysis of stratigraphy: The OxCal program. *Radiocarbon* **37**, 425–430 (1995).

66. C. B. Ramsey, Deposition models for chronological records. *Quat. Sci. Rev.* **27**, 42–60 (2008).

67. M. Ndeye, Marine reservoir ages in northern Senegal and Mauritania coastal waters. *Radiocarbon* **50**, 281–288 (2008).

68. S. Kusch, J. Rethemeyer, E. Schefuß, G. Mollenhauer, Controls on the age of vascular plant biomarkers in Black Sea sediments. *Geochim. Cosmochim. Acta* **74**, 7031–7047 (2010).

69. F. A. Smith, K. H. Freeman, Influence of physiology and climate on δD of leaf wax *n*-alkanes from C_3 and C_4 grasses. *Geochim. Cosmochim. Acta* **70**, 1172–1187 (2006).

70. S. J. Feakins, A. L. Sessions, Controls on the D/H ratios of plant leaf waxes in an arid ecosystem. *Geochim. Cosmochim. Acta* **74**, 2128–2141 (2010).

71. D. Sachse, G. Gleixner, H. Wilkes, A. Kahmen, Leaf wax n-alkane δD values of field-grown barley reflect leaf water δD values at the time of leaf formation. *Geochim. Cosmochim. Acta* **74**, 6741–6750 (2010).

72. S. J. Feakins, Pollen-corrected leaf wax D/H reconstructions of northeast African hydrological changes during the late Miocene. *Palaeogeogr. Palaeoclimatol. Palaeoecol.* **374**, 62–71 (2013).

73. C. R. Magill, G. M. Ashley, K. H. Freeman, Water, plants, and early human habitats in eastern Africa. *Proc. Natl. Acad. Sci. U.S.A.* **110**, 1175–1180 (2013).

74. Y. Garcin, E. Schefuß, V. F. Schwab, V. Garreta, G. Gleixner, A. Vincens, G. Todou, O. Séné, J.-M. Onana, G. Achoundong, D. Sachse, Reconstructing C3 and C4 vegetation cover using n-alkane carbon isotope ratios in recent lake sediments from Cameroon, Western Central Africa. *Geochim. Cosmochim. Acta* **142**, 482–500 (2014).

75. Y. Chikaraishi, H. Naraoka, δ13C and δD relationships among three n-alkyl compound classes (n-alkanoic acid, n-alkane and n-alkanol) of terrestrial higher plants. *Org. Geochem.* **38**, 198–215 (2007).

76. D. P. Schrag, G. Hampt, D. W. Murray, Pore fluid constraints on the temperature and oxygen isotopic composition of the glacial ocean. *Science* **272**, 1930–1932 (1996).

77. L. E. Lisiecki, M. E. Raymo, A Pliocene-Pleistocene stack of 57 globally distributed benthic delta O-18 records. *Paleoceanography* **20**, PA1003 (2005).

78. W. Dansgaard, Stable isotopes in precipitation. *Tellus* **16**, 436–468 (1964).

79. F. Gasse, Diatom-inferred salinity and carbonate oxygen isotopes in Holocene waterbodies of the western Sahara and Sahel (Africa). *Quat. Sci. Rev.* **21**, 737–767 (2002).

80. K. Yoshimura, M. Kanamitsu, D. Noone, T. Oki, Historical isotope simulation using reanalysis atmospheric data. *J. Geophys. Res. Atmos.* **113**, D19108 (2008).

81. A. Gelman, J. Carlin, H. Stern, D. Rubin, *Bayesian Data Analysis* (Chapman & Hall/CRC, ed. 2, 2003).

82. K. Rozanski, L. Araguas-Araguas, R. Gonfiantini, in *Climate Change in Continental Isotopic Records*, P. K. Swart, K. C. Lohmann, J. Mckenzie, S. Savin, Eds. (American Geophysical Union, 1993), vol. 78, pp. 1–36.

83. M. Zhao, N. A. S. Beveridge, N. J. Shackleton, M. Sarnthein, G. Eglinton, Molecular stratigraphy of cores off northwest Africa: Sea surface temperature history over the last 80 ka. *Paleoceanography* **10**, 661–675 (1995).

84. P. deMenocal, J. Ortiz, T. Guilderson, M. Sarnthein, Coherent high-and low-latitude climate variability during the Holocene warm period. *Science* **288**, 2198–2202 (2000).

85. W. S. Broecker, M. Klas, E. Clark, G. Bonani, S. Ivy, W. Wolfli, The influence of CaCO3 dissolution on core top radiocarbon ages for deep-sea sediments. *Paleoceanography* **6**, 593–608 (1991).

86. L. R. Teal, M. T. Bulling, E. R. Parker, M. Solan, Global patterns of bioturbation intensity and mixed depth of marine soft sediments. *Aquat. Biol.* **2**, 207–218 (2008).

87. M. H. Trauth, M. Sarnthein, M. Arnold, Bioturbational mixing depth and carbon flux at the seafloor. *Paleoceanography* **12**, 517–526 (1997).

88. F. Legeleux, J.-L. Reyss, S. Schmidt, Particle mixing rates in sediments of the northeast tropical Atlantic: Evidence from 210Pbxs, 137Cs, 228Thxs and 234Thxs downcore distributions. *Earth Planet. Sci. Lett.* **128**, 545–562 (1994).

89. T. M. Shanahan, J. T. Overpeck, C. W. Wheeler, J. W. Beck, J. S. Pigati, M. R. Talbot, C. A. Scholz, J. Peck, J. W. King, Paleoclimatic variations in West Africa from a record of late Pleistocene and Holocene lake level stands of Lake Bosumtwi, Ghana. *Palaeogeogr. Palaeoclimatol. Palaeoecol.* **242**, 287–302 (2006).

90. M. H. Marshall, H. F. Lamb, D. Huws, S. J. Davies, R. Bates, J. Bloemendal, J. Boyle, M. J. Leng, M. Umer, C. Bryant, Late Pleistocene and Holocene drought events at Lake Tana, the source of the Blue Nile. *Glob. Planet. Change* **78**, 147–161 (2011).

91. K. Costa, J. Russell, B. Konecky, H. Lamb, Isotopic reconstruction of the African Humid Period and Congo air boundary migration at Lake Tana, Ethiopia. *Quat. Sci. Rev.* **83**, 58–67 (2014).

92. J. E. Tierney, J. M. Russell, Y. Huang, J. S. S. Damsté, E. C. Hopmans, A. S. Cohen, Northern hemisphere controls on tropical southeast African climate during the past 60,000 years. *Science* **322**, 252–255 (2008).

93. D. Verschuren, J. S. S. Damsté, J. Moernaut, I. Kristen, M. Blaauw, M. Fagot, G. H. Haug; CHALLACEA Project Members, Half-precessional dynamics of monsoon rainfall near the East African Equator. *Nature* **462**, 637–641 (2009).

94. J. E. Tierney, J. M. Russell, J. S. S. Damsté, Y. Huang, D. Verschuren, Late Quaternary behavior of the East African monsoon and the importance of the Congo Air Boundary. *Quat. Sci. Rev.* **30**, 798–807 (2011).

95. E. Gasse, F. A. Street, Late Quaternary lake-level fluctuations and environments of the northern Rift Valley and Afar region (Ethiopia and Djibouti). *Palaeogeogr. Palaeoclimatol. Palaeoecol.* **24**, 279–325 (1978).

96. R. Gillespie, F. A. Street-Perrott, R. Switsur, Post-glacial arid episodes in Ethiopia have implications for climate prediction. *Nature* **306**, 680–683 (1983).

97. M. Servant, S. Servant-Vildary, *The Sahara and the Nile*, M. A. J. Williams, H. Faure, Eds. (A.A. Balkema, 1980), pp. 133–162.

98. Y. Garcin, D. Melnick, M. R. Strecker, D. Olago, J.-J. Tiercelin, East African mid-Holocene wet–dry transition recorded in palaeo-shorelines of Lake Turkana, northern Kenya Rift. *Earth Planet. Sci. Lett.* **331–332**, 322–334 (2012).

99. P. Hoelzmann, F. Gasse, L. M. Dupont, U. Salzmann, in *Past Climate Variability Through Europe and Africa*, R. W. Battarbee, F. Gasse, C. E. Stickley, Eds. (Springer Netherlands, 2004), pp. 219–256.

100. R. Baumhauer, in *Environmental History and Palaeolimnology*, J. P. Smith, P. G. Appleby, R. W. Battarbee, J. A. Dearing, R. Flower, E. Y. Haworth, F. Oldfield, P. E. O'Sullivan, Eds. (Springer Netherlands, 1991), pp. 347–357.

101. F. Gasse, R. Téhet, A. Durand, E. Gibert, J.-C. Fontes, The arid–humid transition in the Sahara and the Sahel during the last deglaciation. *Nature* **346**, 141–146 (1990).

102. J. C. Stager, B. Cumming, L. Meeker, A high-resolution 11,400-yr diatom record from Lake Victoria, East Africa. *Quat. Res.* **47**, 81–89 (1997).

103. M. A. Berke, T. C. Johnson, J. P. Werne, K. Grice, S. Schouten, J. S. S. Damsté, Molecular records of climate variability and vegetation response since the Late Pleistocene in the Lake Victoria basin, East Africa. *Quat. Sci. Rev.* **55**, 59–74 (2012).

104. F. Gasse, J. C. Fontes, J. C. Plaziat, P. Carbonel, I. Kaczmarska, P. De Deckker, I. Soulié-Marsche, Y. Callot, P. A. Dupeuble, Biological remains, geochemistry and stable isotopes for the reconstruction of environmental and hydrological changes in the Holocene lakes from North Sahara. *Palaeogeogr. Palaeoclimatol. Palaeoecol.* **60**, 1–46 (1987).

Citation: J. E. Tierney, F. S. R. Pausata, P. B. deMenocal, Rainfall regimes of the Green Sahara. *Sci. Adv.* **3**, e1601503 (2017).